Article

Current Biology

Cell Death in Cells Overlying Lateral Root Primordia Facilitates Organ Growth in *Arabidopsis*

Graphical Abstract

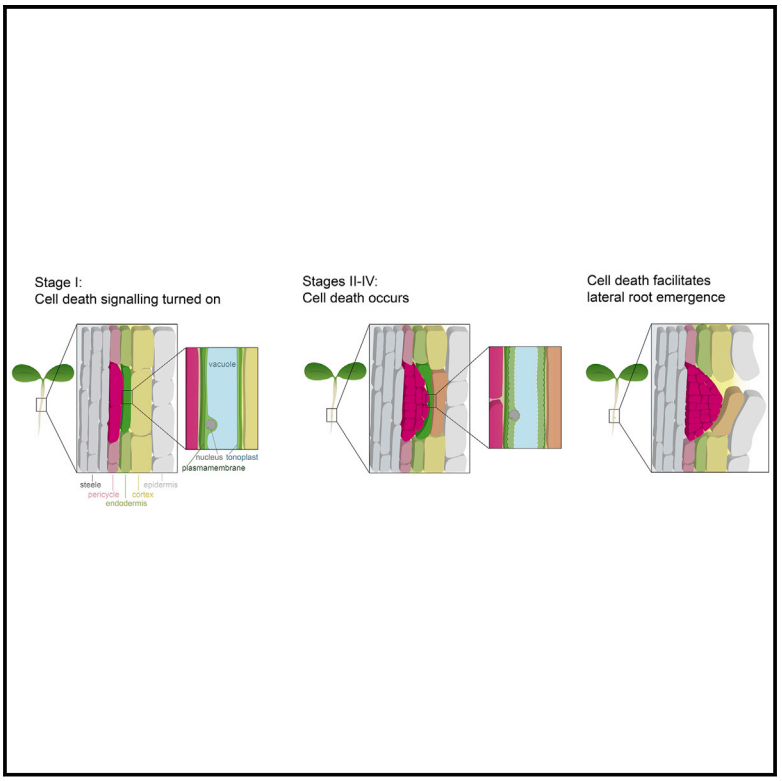

Authors

Sacha Escamez, Domenique André, Bernadette Sztojka, ..., Magnus Andersson, Malcolm Bennett, Hannele Tuominen

Correspondence

hannele.tuominen@umu.se

In Brief

Escamez et al. report that a subset of cells overlying newly formed lateral roots within the parent root dies to facilitate early lateral root organ growth. Our findings suggest that, contrary to common belief, cell death can, as in animals, regulate organ growth in plants, which may have implications for our understanding of evolution.

Highlights

- Growth of lateral root primordia (LRP) coincides with cell death gene expression
- A subset of LRP-overlying cells expresses cell death genes and dies upon LRP growth
- *ore1* mutants deficient in LRP-overlying cell death show delayed LRP growth
- Rescuing cell death in *ore1* via genetics or laser ablation rescues LRP growth

Escamez et al., 2020, Current Biology *30*, 1–10
February 3, 2020
https://doi.org/10.1016/j.cub.2019.11.078

CellPress

Please cite this article in press as: Escamez et al., Cell Death in Cells Overlying Lateral Root Primordia Facilitates Organ Growth in *Arabidopsis*, Current Biology (2019), https://doi.org/10.1016/j.cub.2019.11.078

Current Biology
Article

Cell Death in Cells Overlying Lateral Root Primordia Facilitates Organ Growth in *Arabidopsis*

Sacha Escamez,[1] Domenique André,[1,6] Bernadette Sztojka,[1] Benjamin Bollhöner,[1] Hardy Hall,[1] Béatrice Berthet,[2] Ute Voß,[3] Amnon Lers,[4] Alexis Maizel,[2] Magnus Andersson,[5] Malcolm Bennett,[3] and Hannele Tuominen[1,6,7,*]
[1]Umeå Plant Science Centre, Department of Plant Physiology, Umeå University, 901 87 Umeå, Sweden
[2]Center for Organismal Studies (COS), University of Heidelberg, Im Neuenheimer Feld 230, 69120 Heidelberg, Germany
[3]Centre for Plant Integrative Biology, University of Nottingham, Nottingham LE12 SRD, UK
[4]Department of Postharvest Science of Fresh Produce, Agricultural Research Organization, Volcani Center, Rishon LeZion, 7528809, Israel
[5]Department of Physics, Umeå University, 901 87 Umeå, Sweden
[6]Present address: Umeå Plant Science Centre, Department of Forest Genetics and Plant Physiology, The Swedish University of Agricultural Sciences, 901 83 Umeå, Sweden
[7]Lead Contact
*Correspondence: hannele.tuominen@umu.se
https://doi.org/10.1016/j.cub.2019.11.078

SUMMARY

Plant organ growth is widely accepted to be determined by cell division and cell expansion, but, unlike that in animals, the contribution of cell elimination has rarely been recognized. We investigated this paradigm during *Arabidopsis* lateral root formation, when the lateral root primordia (LRP) must traverse three overlying cell layers within the parent root. A subset of LRP-overlying cells displayed the induction of marker genes for cell types undergoing developmental cell death, and their cell death was detected by electron, confocal, and light sheet microscopy techniques. LRP growth was delayed in cell-death-deficient mutants lacking the positive cell death regulator ORESARA1/ANAC092 (ORE1). LRP growth was restored in *ore1-2* knockout plants by genetically inducing cell elimination in cells overlying the LRP or by physically killing LRP-overlying cells by ablation with optical tweezers. Our results support that, in addition to previously discovered mechanisms, cell elimination contributes to regulating lateral root emergence.

INTRODUCTION

In contrast to that in animals [1], cell elimination is generally considered not to play a role in regulating plant organ growth [2–4]. Cell elimination occurs frequently as part of plant development in a genetically controlled manner often referred to as programmed cell death (PCD) [5, 6], as evidenced by the expression of a particular set of genes specifically in cells that are bound to undergo developmental cell elimination [7]. Cell death and the subsequent cell degradation are usually considered cell autonomous, as during the formation of water-conducting xylem tracheary elements (TEs) [8] or the elimination of lateral root cap cells that surround the root tip and regulate root growth [9]. Nevertheless, developmentally regulated cell elimination can also rely on non-cell-autonomous mechanisms [10], as in the *Arabidopsis* endosperm, where the core developmental cell death indicator genes [7] are induced, but where cell death itself is caused by pressure from the growing embryo into the location of the endosperm [11]. The fact that different mechanisms have been co-opted to control developmental cell elimination supports that cell elimination plays several crucial roles during development, suggesting a more prominent role during plant organ growth than previously thought.

Morphological features of cell death have been observed in several species in cells overlying the sites of lateral root (LR) formation within existing roots [12–15]. The lateral roots are initiated from a subset of pericycle cells that form the LR primordium (LRP) deep in the parent organ [16, 17]. The developing LRP must therefore traverse the overlying endodermal, cortical, and epidermal cell layers for LR emergence (LRE) to occur. LRE has been shown to rely on cell divisions and turgor-driven expansion in the LRP [16, 18], as well as on changes in the cell walls and shapes of the LRP-overlying cells [18–24]. Cell death is not believed to occur during LRE in *Arabidopsis* [25, 26], and the cell death reported in the LRP-overlying cells of other species [12–15] has not been studied in relation to LRP growth, leaving open the question of whether cell death contributes to LRE.

In *Arabidopsis*, the most dramatic changes reported during LRE occur in the LRP-overlying endodermal cells due to their position in immediate contact with the LRP and the presence of their lignified casparian strip cell wall region. In front of the growing LRP, endodermal cells modify their shape to such an extent that they occasionally split, with both halves having the ability to maintain plasma membrane integrity at least for some time [23]. The cortical and epidermal cells are less affected, as their cell walls are loosened by hydrolytic enzymes so that they can separate to allow the emerging LRP to pass through [19, 26]. There is no report of cell death during LRE in *Arabidopsis*, suggesting that the remodeling and separation of the LRP-overlying cells are sufficient to ensure LRE without any contribution from cell death. However, cysteine proteases associated with cell death and autolysis are expressed in LRP-overlying cells [27], supporting the occurrence of cell death during LRE in *Arabidopsis*.

The present study investigates whether cell death occurs in the LRP-overlying cells during LRE in *Arabidopsis*, and if so, whether it contributes to LRP growth. We detected the expression of several canonical marker genes for developmental cell death [7] in a subset of LRP-overlying cells. Electron microscopy revealed the autolytic features indicative of cell death in endodermal cells overlying early-stage LRPs. Combined viability and cell death stains also indicated the presence of dead LRP-overlying cells before the LRP had crossed any overlying cell layers. Live cell imaging by confocal and light sheet microscopy confirmed that cell death occurred in a subset of the LRP-overlying endodermal cells, concomitant with the growth of the LRP through the endodermis. Plants unable to express ORESARA1/ANAC092 (ORE1), a transcription factor contributing to the transcriptional activation of several cell death-related genes [28], displayed the decreased cell death of LRP-overlying cells as well as a delay in LRE. When cell death was restored in the overlying cells of these plants by either expressing the mammalian cell death-promoting factor mBAX [29–31] or using laser-assisted targeted cell elimination (hereafter called laser ablation) inspired by previous studies [32–35], LRP growth reverted to normal, indicating that cell elimination contributes to the regulation of organ growth during LRE.

RESULTS

Cell Death Indicator Genes Are Induced in Cells Overlying LRP

In a time-course transcriptomics dataset covering various stages of LRP growth [36], we detected the upregulation of *BIFUNCTIONAL NUCLEASE 1* (*BFN1*), which functions in cell autolysis associated with developmental cell death [9] (Table S1). Several other genes belonging to the set of transcriptional reporters for cell types undergoing developmental cell death and autolysis [7] were identified among the genes most correlated with *BFN1* in the LRE transcriptome. Among them, *METACASPASE 9* (*MC9*), *RIBONUCLEASE 3* (*RNS3*), *EXITUS 1* (*EXI1*) and *DUF679 DOMAIN MEMBRANE PROTEIN 4* (*DMP4*), together with *BFN1*, represent five of the nine core marker genes specifically expressed in cell types undergoing developmental cell death in *Arabidopsis* [7] and are hereafter referred to as "cell death indicator genes" (Figure 1A; Table S1). Using promoter::*GUS* reporter lines, we also detected the activation of the promoters of these cell death indicator genes in LRP-overlying cells at different stages of LRP growth (Figure 1B), defined according to Malamy and Benfey [16].

A more detailed time-lapse confocal microscopy analysis of a pro*BFN1::*nuc*GFP* reporter line [37] carrying the pro*UBQ10::WAVE131*:*YFP* plasma membrane marker [38] indicated *BFN1* promoter activity in an endodermal cell overlying an early-stage LRP and revealed the apparent loss of nuclear integrity at stage III (Figure 1C). Overall, for 381 observed LRP, induction of the pro*BFN1::*nuc*GFP* reporter was detected in at least 1 LRP-adjacent cell (i.e., overlying the LRP during early stages of LRP growth or neighboring the LRP in late stages of growth) 53.5% of the time in the endodermis, 14.7% of the time in the cortex, and 9.7% of the time in the epidermis. These averages likely underestimate the actual frequency of cell death indicator gene expression because transcriptional markers for the activation of cell death disappear upon the execution of cell death. When considering cell death indicator gene expression in relation to LRP stage, the frequency of pro*BNF1::*nuc*GFP* signal adjacent to an LRP reached >90% in the endodermis at stage IV, nearly 50% in the cortex at stage VII, and 38% in the epidermis at stage VII (Figures 1D and 1E). These results indicate that over the course of LRP growth, there is almost always a time when a cell death indicator gene is induced in at least one LRP overlying endodermal cell and also, although less frequently, in adjacent cortical and epidermal cells.

Cell Death Occurs in a Subset of LRP-Overlying Cells

To determine the fate of the cells overlying the growing LRP, we used several cell-death-detection methods. The previously published tonoplast integrity marker (ToIM) results in a GFP signal in the cytoplasm and nucleus as well as a red fluorescent protein (RFP) signal in the vacuole of viable cells, while both signals mix and GFP rapidly quenches upon tonoplast rupture and cytoplasmic acidification that result from cell death [9]. This cell death marker driven by the *BFN1* promoter (pro*BFN1::ToIM*) indicated the occurrence of cell death in xylem TEs known to undergo developmental cell death [37] as well as in a subset of LRP-adjacent cells (Figures 2A, S1A, and S1B). Activation of autophagy, a cellular process that has been linked to developmental cell death [39–42], could also be visualized in a subset of overlying cells (Figure S1C) by detecting the autophagy marker GFP:ATG8a driven by the *ATG8a* endogenous promoter [43]. Furthermore, seedlings were stained simultaneously with the viability marker fluorescein diacetate (FDA), which fluoresces in living cells but not in dead cells, and with propidium iodide (PI), which is normally excluded from living cells [44, 45] (Figure 2B). The absence of an FDA signal combined with PI entry (Figures 2B and 2C) indicated that cell death occurred specifically in a subset of endodermal and cortical cells overlying LRP at early stages (stages I to IV, before crossing of the endodermis).

Transmission electron microscopy (TEM) observations on root cross-sections (Figure 2D) showed plasmolysis and autolytic features indicative of cell death, such as leakage of intracellular material outside the protoplast, specifically in cells overlying even early-stage LRP (Figures 2E–2I). These TEM observations are therefore consistent with the occurrence of cell death and autolysis in a subset of LRP-overlying cells in the endodermis (Figures 2E–2I) before the LRP crossing this cell layer.

The observation of cell death-related features in LRP-overlying endodermal cells (Figures 2B–2I), together with the high frequency of *BFN1* transcriptional activation in the endodermis (Figure 1D), prompted us to observe endodermal cells by time-lapse confocal and light sheet microscopy using the endodermis-specific plasma membrane marker pro*CASP1::CITRINE:SYP122* [23], together with the pro*BFN1::*nuc*GFP* cell death marker. This latter marker not only reveals transcriptional activation of cell death indicator genes but also can indicate cell death execution, based on the abrupt disappearance of the nuclear GFP signal known to shortly follow cell death [9, 37]. Time-lapse confocal microscopy imaging of LRP provided evidence for the occurrence of cell death in endodermal cells overlying LRP, as revealed by the complete loss of the nuclear GFP signal in these endodermal cells between two consecutive time points (Figures

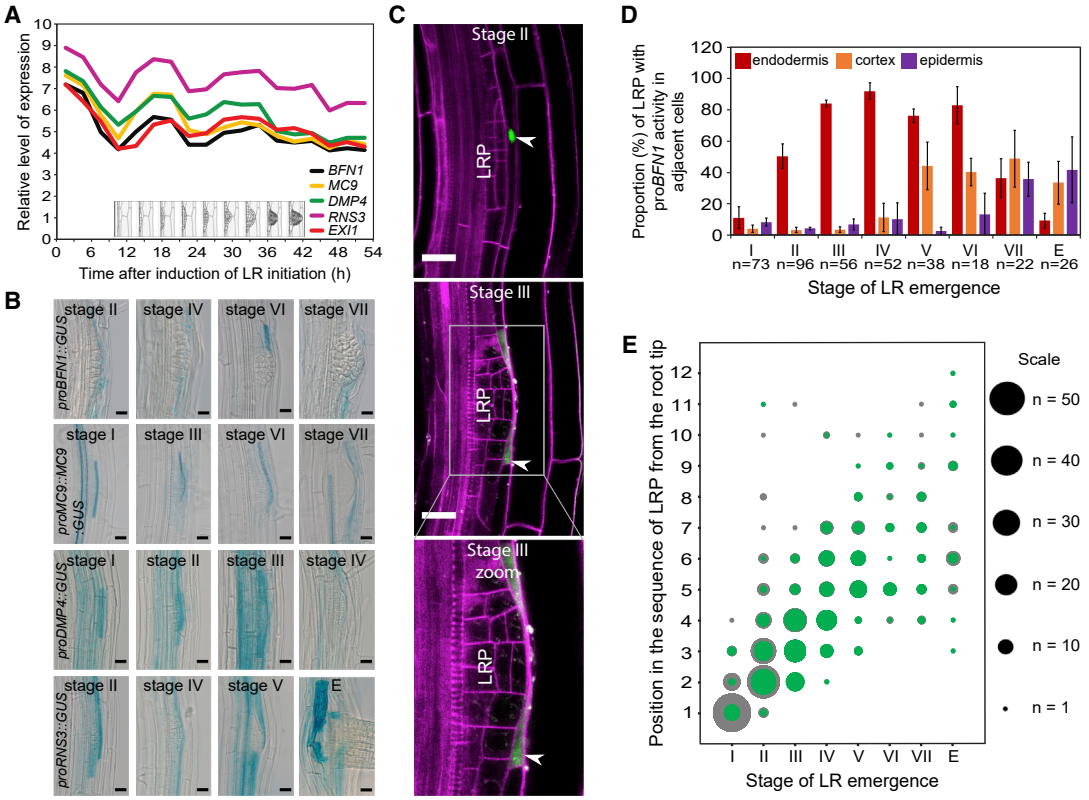

Figure 1. Transcriptional Activation of Cell Death Indicator Genes in LRP-Overlying Cells

(A) Expression profile of *BFN1* and four highly correlated cell death indicator genes in the lateral root (LR) development time course transcriptomics dataset from [36]. The five cell death indicator genes display three peaks of expression coinciding temporally with the passage of the growing LRP through each of the three overlying (endodermal, cortical, and epidermal) cell layers. See also Table S1 and Video S4.

(B) Promoter activity profile of the cell death indicator genes *BFN1*, *MC9*, *DMP4*, and *RNS3* in the tissues overlying naturally initiated LR primordia (LRP) at the indicated stages. Bars, 25 μm. Note that in addition to signal in the overlying cells, there is often signal in the protoxylem vessel.

(C) Micrographs of confocal laser scanning microscopy imaging of pro*BFN1::nucGFP* expression (green) and ubiquitous plasma membrane marker pro*UBQ10::WAVE131:YFP* (magenta) around LRP. Arrowheads indicate GFP$^+$ nuclei adjacent to the developing LRP. The lowest panel is a magnification of the highlighted area of the middle panel, showing GFP in the entire cytoplasm of a squeezed endodermal cell, indicating loss of nuclear integrity. Bars, 20 μm.

(D) Proportion of LRP displaying nuclear GFP signal in at least one LRP adjacent endodermal cell (red), cortical cell (orange), or epidermal cell (purple), for each stage of LRP development in the pro*BFN1::nucGFP* seedling roots. Values represent the averages of three replicate experiments, each including 20 seedlings and >100 primordia. The total number of LRP observed at each stage (across all three replicate experiments) is indicated. Error bars indicate SEMs.

(E) Visualization of LRP stage distribution in terms of LRP sequence from the root tip of 60 5- to 6-day-old *Arabidopsis* seedlings. The size of each dot is proportional to the number of observed LRP at each stage and position in total (gray) or with at least one pro*BFN1::nucGFP*$^+$ overlying cell (green). E, emerged.

2J, 2K, and S1D–S1H). Light sheet microscopy (which provided a 12-fold greater time resolution) revealed the complete disappearance of the nuclear GFP signal between two consecutive time points in the LRP-overlying endodermal cells (Figure 2L; Videos S1 and S2). One of these endodermal nuclei disintegrated just before losing its signal (Figure 2L; Video S1). Both the apparent nuclear disintegration and the rapidity of the nuclear signal disappearance can be explained only by cell death. The shapes of the plasma membranes of the LRP-overlying cells at the times of death indicated that the LRP had not yet entirely traversed the endodermis (Figures 2J, 2L, and S1D–S1H; Video S3), meaning that the observed cell death events occurred either before or during the passage of the LRP through the endodermal layer. A very limited number of surviving endodermal cells in close proximity to LRP displayed a slow and gradual decrease in the nuclear GFP signal (Figures S1D–S1H), suggesting deactivation of the cell death and autolysis transcriptional machinery in these cells. A few other endodermal cells kept a high level of nuclear GFP signal over the observation time span (Figures 2L and S1D–S1H), and it is possible that these cells died at a later point during LRP emergence.

Cell Death in LRP-Overlying Cells Facilitates LRP Growth

We reasoned that if cell death played a role in facilitating LRP growth, then plants impaired in parts of the cell death machinery may show delayed LRE. To compare the speed of LRE between genotypes, LR initiation was induced synchronously by gravitational stimulus (90° rotation of the seedlings) [16, 18]. When monitored at 18 and 42 h post-gravitational induction (pgi), the single mutants for the cell death indicator genes did not show any consistent or significant changes in LRP growth (Figure S2), possibly because of functional redundancy, which is a common problem when studying plant cell death [46].

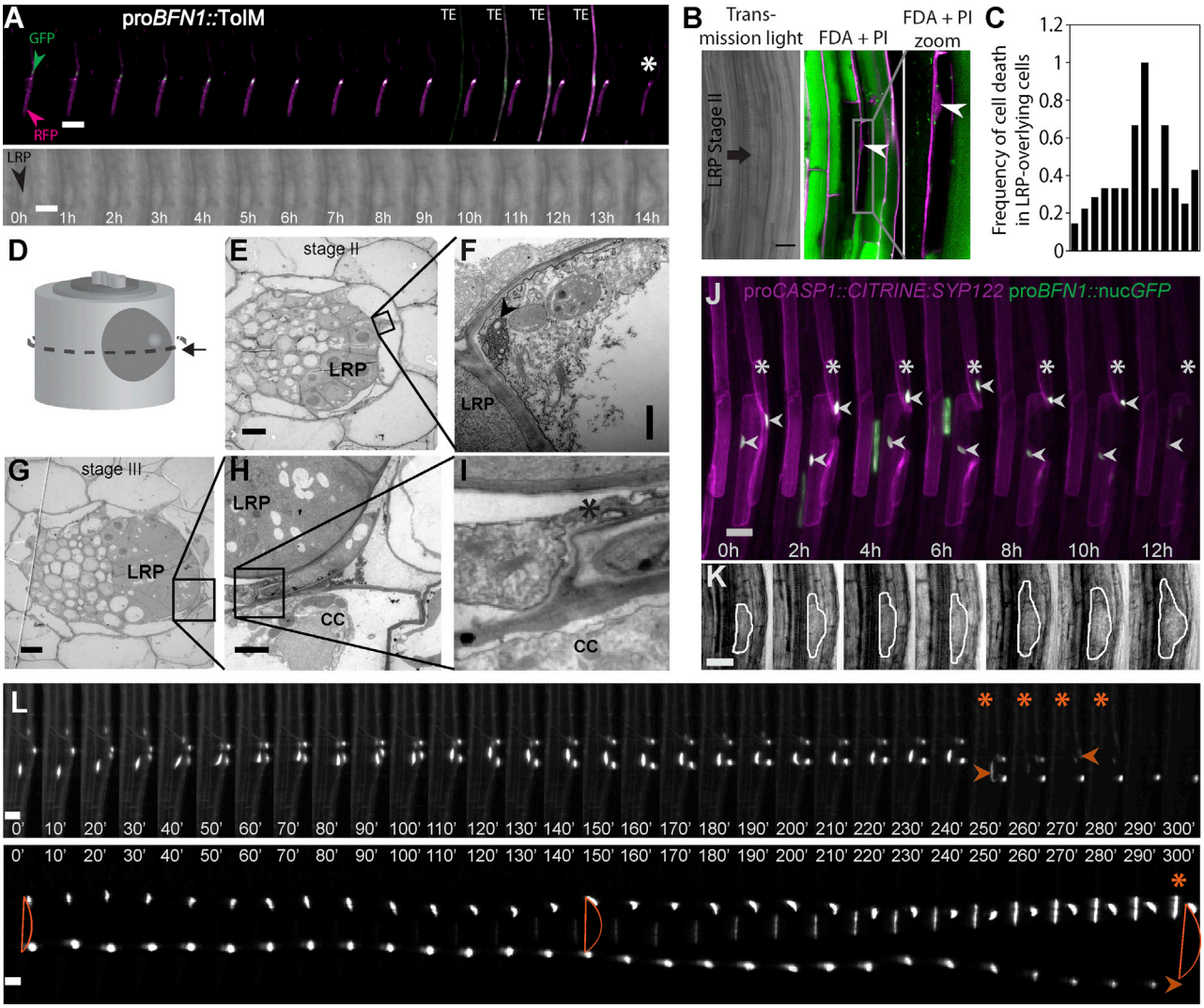

Figure 2. Detection of Cell Death in LRP-Overlying Cells

(A) The top panel displays a time-lapse confocal microscopy 3D projection of pro*BFN1::TolM* (tonoplast integrity marker, consisting of cytoplasmic and nuclear GFP as well as vacuolar RFP [9]) fluorescence in a cell overlying a naturally occurring LRP. The bottom panel shows the transmission light, where the LRP can be distinguished. Arrowheads mark the indicated fluorophores and the asterisk marks the loss of GFP signal, which reveals cell death. TE, xylem tracheary element, known to undergo canonical developmental cell death. Bars, 50 μm. See also Figures S1A and S1B and Video S4.

(B) Cell death detection relying on the absence of viability staining fluorescein diacetate (FDA) signal (green) and on nuclear staining propidium iodide (PI, magenta) observed with confocal laser scanning microscopy imaging of LRPs and their overlying cells in the main roots of 4- to 5-day-old *Arabidopsis* seedlings. White arrowhead points at an endodermal cell displaying signs of cell death (absence of FDA combined with PI entry).

(C) Frequency of cell death observed by double staining (y axis), as in (B), in cortical and endodermal cells overlying LRP at stages I to IV in 4- to 5-day-old Col-0 WT in 13 independent experiments (each bar represents the mean of each independent experiment).

(D–I) TEM of cross-sections through an LRP and the surrounding tissues. The position of the cross-section within the root is shown in (D). Stage-II (E and F) and stage-III (G–I) LRPs are shown. (F) is a magnification from (E). (I) is a magnification of (H), which itself is a magnification of (G). The arrowhead indicates the apparent loss of plasma membrane integrity, while the asterisk indicates leakage of intracellular material. CC, cortical cell. Bar, 5 μm (E and G), 2 μm (H), and 0.5 μm (I).

(J) Time-lapse confocal microscopy 3D projection of the endodermal plasma membrane marker pro*CASP1::CIT:SYP122* (purple) and the nuclear cell death reporter pro*BFN1::nucGFP* (green) around a developing LRP. The asterisks mark the endodermal cell, which ultimately dies (between 10 and 12 h), while the arrowheads point at the endodermal nuclei displaying the GFP signal. The elongated area with the GFP signal seen in the stele from 2 to 6 h is the nucleus of a xylem TE undergoing developmental cell death and autolysis. Bar, 25 μm. See also Figure S1D–S1H.

(K) Transmission light images corresponding to the images in (J). The LRP are highlighted by white lines. Bars, 25 μm.

(L) Montage of 3D projection from light sheet microscopy time-lapse imaging of the endodermal plasma membrane marker pro*CASP1::CIT:SYP122* and the nuclear-localized cell death indicator gene transcriptional reporter pro*BFN1::nucGFP* around a developing LRP. The two rows show two different primordia (each from an independent seedling). In the top panel, the presence of an LRP can be deduced from the bent shape of the overlying endodermal cells, while in the bottom panel, the relative weakness of the plasma membrane compared to nuclear fluorescence makes it necessary to indicate the LRP shape with orange lines. Asterisks indicate time points when an endodermal nucleus is seen to disintegrate or disappear. Arrowheads point at disintegrating nuclei. Bars, 20 μm. See also Videos S1, S2, and S3.

A large number of cell death-related genes, including the five cell death indicators co-expressed during LRE, are transcriptionally regulated by, among other regulators, the NAC transcription factor ORESARA1/ANAC092 (ORE1) [28]. ORE1 is known to regulate the genes associated with hormones, cell wall remodeling, and cell death, and it is expressed in connection with several types of developmental cell death and autolysis [47, 48]. Furthermore, *ORE1* overexpression was previously reported to increase LR number, while knocking it out did not decrease the number of formed LR [49], even if these LR seemed shorter [49]. We detected *ORE1* promoter [28] activity in roots, including LRP-overlying cells (Figure S3A). This is consistent with the transcriptomics study over time on sections of roots induced to develop an LRP [36], in which *ORE1* shows overall strong expression. The expression of *ORE1* in LRP-overlying cells is compatible with a potential role for ORE1 in the transcriptional control of cell death in the LRP-overlying cells. We therefore hypothesized that analyzing LRP growth in *ore1* mutants could overcome potential genetic redundancies between cell death-related genes during LRE.

Consistent with a role for ORE1 during LRE, shorter LRs and fewer emerged LRs were observed in two *ore1* mutant alleles compared to wild-type (WT) seedlings (Figures S3B–S3D). Gravitational induction experiments confirmed that LRP growth was delayed in these *ore1* mutants compared with WT (Figure 3A), and even without synchronous induction, *ore1-2* had significantly fewer emerged LRs than WT (Figure 3B). Furthermore, simultaneous FDA and PI staining showed significantly less frequent cell death in the LRP-overlying cells of *ore1-2* than in WT (Figures 3C and 3D). The fact that cell death was strongly reduced in *ore1-2* compared with WT, but not completely abolished, indicates that ORE1 is not the sole regulator of LRP-overlying cell death. Nevertheless, the strong reduction in overlying cell death in this mutant (Figures 3C and 3D), concomitant with the reduced speed of LRP growth (Figures 3A and 3B), justify using the *ore1-2* mutant as a tool to test a possible relation between LRP growth speed and overlying cell death.

To test whether loss of *ORE1* expression correlated with slower LRP growth as a result of less frequent cell death in the overlying cells, we set out to rescue the LRE delay of *ore1-2* by inducing cell death in cells overlying LRP (genetic rescue strategy; Figures 3B–3D) or by mortally wounding LRP-overlying cells by laser ablation (physical rescue strategy; Figures 4A–4D).

For the genetic rescue strategy, we expressed the pro-apoptotic mammalian protein mBAX [29], known to potently induce cell death in *Arabidopsis* [30, 31], under the transcriptional control of the *BFN1* promoter (pro*BFN1::mBAX*) in the *ore1-2* background. The use of the *BFN1* promoter is justified because the promoters of the cell death indicator genes such as *BFN1* are the only ones known to be active specifically in the subset of LRP-overlying cells that die during LRE. Despite the regulation of *BFN1* by ORE1 [28], *BFN1* expression in the *ore1-2* background has previously been shown to be reduced, but not abolished [48]. Furthermore, the reduced, rather than the abolished, cell death frequency in LRP-overlying cells of *ore1-2* (Figures 3C and 3D) strongly suggests that the *BFN1* promoter retains some activity in LRP-overlying cells in *ore1-2*. Consistently, we found that the *BFN1* promoter activity in the *ore1-2* mutant was still sufficient to drive the expression of *mBAX* in the *ore1-2* pro*BFN1::mBAX* lines (Figures S3E and S3F). In addition, the *BFN1* promoter is specific for cells bound to undergo developmental cell death [7], meaning that the use of the *BFN1* promoter to drive mBAX expression is not expected to result in the death of cells that should not die, and therefore to result in a WT-like phenotype in both *ore1-2* and WT backgrounds (Figure S3G).

While LR density was reduced in upright grown 7-day-old *ore1-2* seedlings compared with Col-0 WT (Figures 3B and S3B–S3D), several *ore1-2* pro*BFN1*::*mBAX* lines that we generated showed similar LR densities as WT, while the others showed a variety of pleiotropic phenotypes such as stunted root growth (Figure 3B). Therefore, we focused on the three *ore1-2* pro*BFN1*::*mBAX* lines (1, 4, and 6) with high mBAX expression (Figure S3E), whose main root growth was not impaired (Figure 3B) and that rescued the *ore1-2* LRP growth delay (Figure 3B). These three *ore1-2* pro*BFN1*::*mBAX* lines displayed LRP-overlying cell death as frequently as in WT (lines 1 and 4) or at even higher (line 6) levels (Figures 3C and 3D), demonstrating the potency of pro*BFN1::mBAX* to induce cell death in LRP-overlying cells, even in the *ore1-2* background. Gravitational induction of *ore1-2* pro*BFN1::mBAX* lines 1 and 4 along with *ore1-2* and WT (Figure 3E) confirmed that the rescue of LRP-overlying cell death in the *ore1-2* background (Figures 3C and 3D) was concomitant with the rescue of LRP growth speed in this mutant (Figure 3E).

For the physical rescue strategy, the junction between an LRP-overlying endodermal cell and its neighboring cortical cell was targeted (to avoid possible damage in the LRP) with optical tweezers to inflict a wound, ultimately leading to the death of the targeted cells (laser ablation) (Figure 4A). The targeted cells showed signs of damage and death within 3 h after laser ablation (Figures 4B and 4C). When laser ablation was performed 24 h after gravitational induction, when the LRP had not yet crossed the endodermis (Figure 4D), the LRP growth became significantly faster and less variable in ablated *ore1-2* than in untreated *ore1-2* (Figure 4D). This partial rescue of LRP growth speed in *ore1-2* following laser ablation of overlying cells confirms that the slower LRP growth in *ore1-2* results from defective cell death in LRP-overlying cells.

DISCUSSION

Our study demonstrates that developmentally regulated cell death occurs in cells overlying LRP in *Arabidopsis* and contributes to regulating LRP growth. Previous studies have shown that living LRP-overlying cells undergo a number of major cell wall and cell shape changes, which also contribute to LRP growth [18–24]. Cell death is therefore one of the mechanisms involved in the regulation of LRP growth in *Arabidopsis*. Regulation of LRP growth by overlying cell death is probably not restricted to *Arabidopsis* because morphological studies indicate the demise of cells overlying LRP in other species such as maize, field bindweed, and soybean [12–15].

The mechanism of cell death in LRP-overlying cells is not known and its execution may differ from other instances of developmental cell elimination, as suggested by the spreading of pro*BFN1*-driven nuclear GFP signal into the entire protoplast of

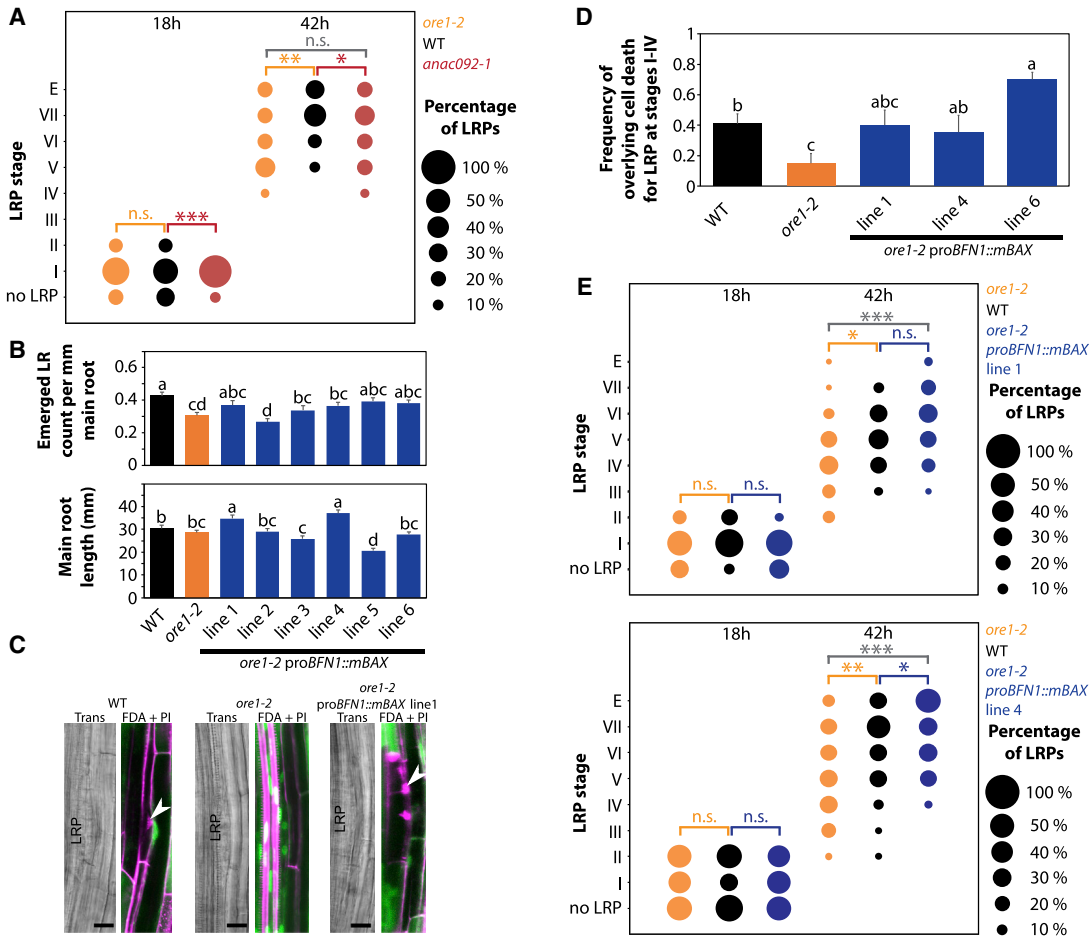

Figure 3. LRE Is Delayed by Loss of the Positive Cell Death Regulator ORE1 and Rescued by Inducing Cell Death in Overlying Cells

(A) Distribution of observed LRP stages 18 and 42 h after gravitational induction of LR initiation in WT and two mutant alleles for *ORE1* (n = 30 observed seedlings). See also Figures S2 and S3A–S3D.

(B) Number of LRs per mm of main root (i.e., emerged LR density) and average total length of the main root from 7-day-old seedlings. Each bar represents the average of 8 replicate experiments (n = 32: 8 experiments × 4 biological replicates per genotype), while the error bars represent SEMs. Similar results were obtained in another set of 8 replicate experiments. The genotypes were compared by post-ANOVA Fisher test. Genotypes that do not share any letter are significantly different from one another. See also Figures S3C–S3G.

(C) Representative 3D projections of double staining with viability dye FDA signal (green) and PI (magenta) observed by confocal laser scanning microscopy imaging of stage II LRPs (seen in transmission light [Trans]) and their overlying cells in the main roots of 4- to 5-day-old *Arabidopsis* seedlings of the indicated genotypes. White arrowhead points at an endodermal cell displaying signs of cell death (absence of FDA signal and PI entry). Bars, 20 μm.

(D) Frequency of cell death observed by double staining, as in (C), in cortical and endodermal cells overlying LRP at stages I–IV, before crossing of the endodermis. Bars represent the average of 4 (mBAX-expressing lines) to 13 (WT and *ore1-2*) replicate experiments, and error bars represent SEMs. The genotypes were compared by post-ANOVA Fisher test. Genotypes that do not share any letter are significantly different from one another.

(E) Distribution of observed LRP stages 18 and 42 h after gravitational induction of LR initiation in WT, *ore1-2* mutant, and *ore1-2* expressing the cell-death-inducing mBAX protein under the transcriptional control of the *BFN1* promoter (20 < n < 33 observed seedlings per genotype). This gravitational induction experiment was repeated 5 times for line 1 and 2 times for line 4.

In (A) and (E), each line was compared with the corresponding WT by Pearson's chi-square test, to reveal potential differences in the distribution of LRP stages dependent on genotype (n.s., not significant, *$p < 0.05$, **$p < 0.01$, ***$p < 0.001$).

an LRP-overlying endodermal cell (Figure 1C). A non-canonical cell death execution in LRP-overlying cells is also supported by the fact that only five of the nine canonical *Arabidopsis* developmental cell death indicator genes [7] were highly co-expressed during LRE (Figure 1A; Table S1). In addition, expression of a ToIM [9] under the control of the *BFN1* promoter revealed a longer time gap between transcriptional activation of this promoter and loss of tonoplast integrity in LRP-overlying cells than in xylem TEs (Video S4), which undergo a well-studied case of developmental cell death and autolysis [8].

The exact spatial and temporal characterization of cell death during LRE is challenging since it is not possible to record the entire time span of LRP growth while using an appropriate chronological resolution to record all cell death events. Our observations over limited time spans or at single time points with stringent criteria (e.g., double staining FDA + PI) necessarily

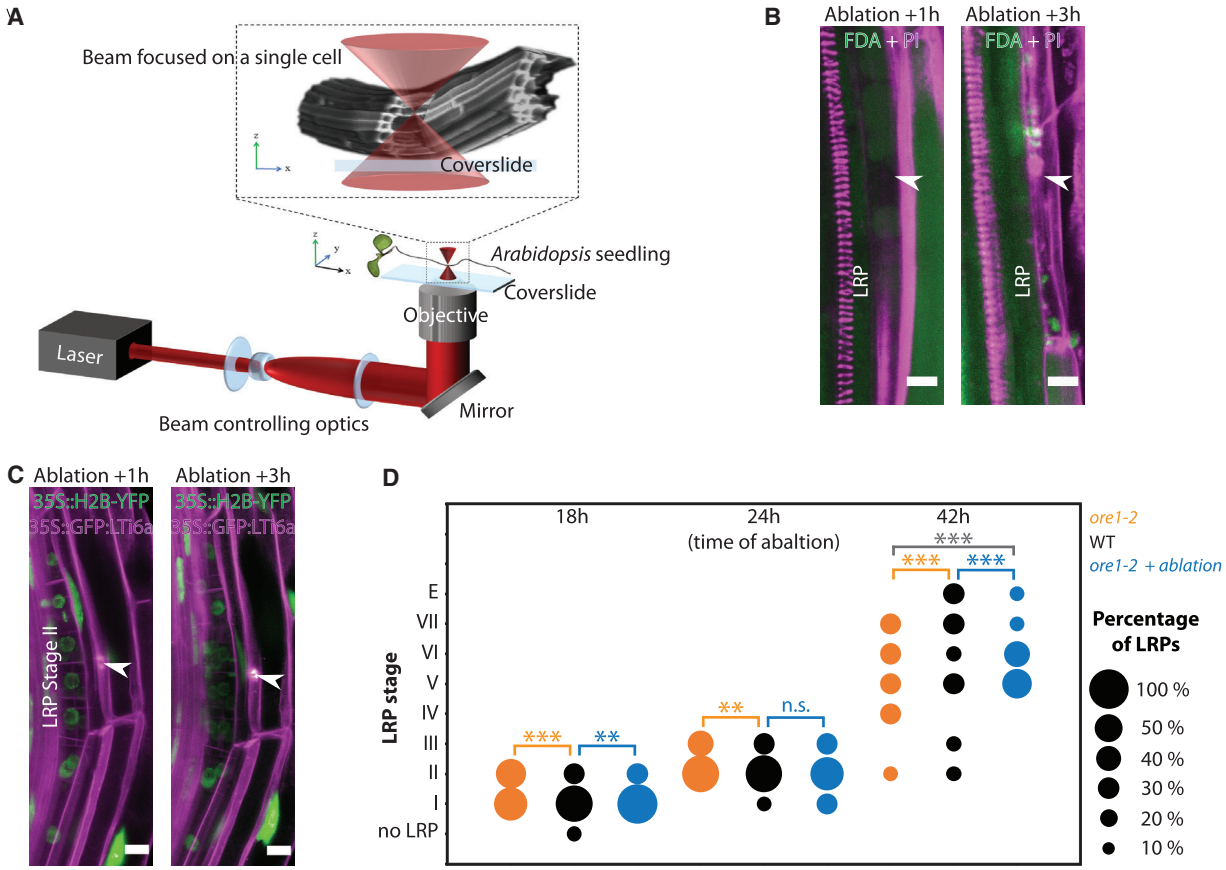

Figure 4. Cell Ablation of LRP-Overlying Cells in Plants Lacking ORE1 Rescues LRE

(A) Schematic illustration of the optical tweezer setup used to specifically target LRP-overlying cells for ablation.

(B) Cell death detection relying on the absence of viability staining FDA signal (green) and on nuclear staining PI (magenta) observed with confocal laser scanning microscopy imaging of LRPs and their overlying cells in the main root of a 4-day-old *Arabidopsis* seedling, 1 or 3 h after laser ablation. White arrowheads point at an endodermal cell targeted for ablation. To avoid possible wounding of the LRP, the side of the endodermal cell toward the cortex was targeted with the laser beam. Both the targeted endodermal cell and the adjacent cortical cell show signs of cell death after 3 h. Scale bars represent 10 μm.

(C) 3D projection of confocal laser scanning micrographs of a stage II LRP and the overlying cells in the main root of a 4-day-old *Arabidopsis* seedling expressing ubiquitously (35S-promoter driven) the plasma membrane marker GFP:LTi6a (magenta) and the nuclear marker H2B:YFP (yellow fluorescent protein; green) 1 and 3 h after targeting an LRP-overlying cell (arrowheads) for laser ablation. After 1 and 3 h, the targeted LRP-overlying cell shows (arrowhead) disorganized plasma membrane at the site where the optical tweezers hit. After 3 h, the damaged area seemed more affected than at 1 h, while the nucleus of the corresponding endodermal cell showed an unusual shape and position (i.e., not pushed against the plasma membrane, despite turgor pressure and the growing LRP). Scale bars represent 10 μm.

(D) Distribution of observed LRP stages 18, 24 (time of ablation), and 42 h after the gravitational induction of LR initiation in WT and *ore1-2* having undergone ablation (or no ablation as a control) of an LRP-overlying endodermal cell (n = 9 observed seedlings from 3 independent experiments). Statistical comparisons correspond to Pearson's chi-square tests, to reveal potential differences in the distribution of LRP stages dependent on genotype (n.s., not significant, *$p < 0.05$, **$p < 0.01$, ***$p < 0.001$).

See also Figures S3B–S3D and S3G.

underestimate the actual frequency of cell death. Such underestimation of cell death frequency is supported by the fact that cell death indicator genes were almost always induced at some point over the course of LRP development (Figure 1D) and by the strong pro*BFN1::*nuc*GFP* signal that persisted in LRP-overlying cells beyond the end of our limited observation time frames (Figures 2L and S1D–S1H). It is therefore likely that overlying cell death would occur in most LRE events when considering the entire time span of LRP growth. The distribution of cell death indicator gene activation over time (Figures 1D and 1E) in relation to the time of cell death execution (Figures 2A, 2J, 2L, and S1D–S1H) suggests the existence of a switch or threshold leading to the execution of cell death. It is therefore possible that the LRP-overlying cell death would follow a bistable switch regulation, whereby a certain threshold of pro-cell death signal determines the commitment to cell death execution, as has recently been shown for the cell death of xylem TEs [50].

Possibly contributing to a bistable-switch regulation, mechanical forces can be expected to influence the fate of the LRP-overlying cells. Strong mechanical pressure is likely to be exerted by the LRP growing against the overlying cells, which themselves alter their mechanical properties and rigidity in coordination

with LRP growth [18, 20]. This could eventually result in the developmentally regulated, non-cell-autonomous death of some weakened overlying cells under intense pressure. Such a scenario is analogous to the elimination of *Arabidopsis* endosperm cells, which, by loosening their cell walls, allow the embryo to grow into the space that they occupy and then mechanically kill them [11]. Similarly, during adventitious root formation, mechanical pressure has been reported to induce cell death in the epidermis of rice in an ethylene-dependent manner [51]. It is therefore possible that mechanical pressure represents at least one of the mechanisms involved in cell death signaling, or even in the execution of cell death itself [10], during LRP growth. Furthermore, such LRP-mediated mechanical pressure would likely affect the overlying cells differently, depending on their own mechanical properties and on their degree of overlap with the growing LRP, which is in line with our observation that only a subset of the LRP-overlying cells dies.

It is possible that the death of a subset of overlying cells facilitates the growth of the LRP by reducing the mechanical resistance of the overlying cells toward the primordia. The plausibility of such a mode of action is supported by the fact that laser ablation of an endodermal cell is potent enough to trigger cell division in the adjacent pericycle [33], likely because the loss of mechanical feedback from the ablated cell allows the necessary swelling of the pericycle to initiate LRP formation [23, 25]. Alternatively, or in addition, cell death may contribute to cell wall remodeling and cell separation and hence to LRP growth by allowing a massive release of cell wall-modifying enzymes and/or of auxin. For example, the cell death of a few columella stem cell daughter cells in *Arabidopsis* roots exposed to low temperature has been shown to affect auxin distribution [52]. Furthermore, the developmental cell death of LR cap (LRC) cells has been shown to result in the release of auxin that is necessary for LR initiation [53]. LRP growth was delayed to a comparable extent in mutants for ORE1 and for the LATERAL ORGAN BOUNDARIES-DOMAIN/ASYMMETRIC LEAVES 2-LIKE29 (LBD29) transcription factor that normally controls auxin accumulation in LRP-overlying cells [21] (Figure 3A versus [21] and Figure S3B). It is therefore tempting to hypothesize that the death of LRP-overlying cells may serve an analogous purpose to LRC cell death in quickly releasing high amounts of auxin for cell wall remodeling of other overlying cells and for LRP growth.

Our finding regarding the impact of cell death on LR growth demonstrates that plant organ growth can be regulated by cell elimination. It was also recently shown that embryo growth requires cell death of the bordering endosperm [11]. Furthermore, the LRC, forming protective cell layers around the root tip, regulates root organ growth based on the cell death dynamics of LRC cells [9]. These findings, therefore, demonstrate that cell proliferation is not the sole factor determining organ growth in plants and that the regulation of organ growth in plants is not dissimilar from that in animals as previously proposed.

This greater similarity than previously accepted in the regulation of organ growth between animals and plants raises some evolutionary questions. Has cell elimination arisen as a mechanism to regulate organ growth from a shared evolutionary heritage between animals and plants, for example, from the regulation of early unicellular populations by cell death [54]? Alternatively, could the regulation of organ growth by cell death in animals and plants have stricken roots at different locations in the tree of life, making it a form of convergent evolution that may in the future reveal some form of deep evolutionary constraint linked with cell elimination?

STAR★METHODS

Detailed methods are provided in the online version of this paper and include the following:

- KEY RESOURCES TABLE
- LEAD CONTACT AND MATERIALS AVAILABILITY
- EXPERIMENTAL MODEL AND SUBJECT DETAILS
  - Plant Material
  - Growth conditions
- METHOD DETAILS
  - BFN1 co-expression analysis
  - Cloning and plant transformation
  - Gravitational induction of LRP initiation
  - Confocal Laser Scanning Microscope analyses
  - Transmission electron microscopy
  - Light microscopy
  - Lightsheet fluorescence microscopy
  - Laser-assisted targeted cell elimination
  - RNA isolation and qPCR
- QUANTIFICATION AND STATISTICAL ANALYSIS
  - Statistical analyses
- DATA AND CODE AVAILABILITY

SUPPLEMENTAL INFORMATION

Supplemental Information can be found online at https://doi.org/10.1016/j.cub.2019.11.078.

ACKNOWLEDGMENTS

We thank Joop Vermeer for the pro*CASP1::CITRINE:SYP122* line, Moritz Nowack for the tonoplast integrity marker, Michael Wilson and Kim Kenobi for bioinformatic assistance, and Tobias Dahlberg and Tim Stangner for help with setting up the optical tweezers system so that it works on plant samples. We acknowledge the Umeå Core Facility for Electron Microscopy (UCEM). This work was supported by the Swedish Research Council VR (621-2013-4949), the Swedish Research Council Formas (232-2009-1698), and the Swedish Governmental Agency for Innovation Systems VINNOVA (015-02290), as well as by the Boehringer Ingelheim Foundation and Deutsche Forschungs gemeinschaft (FOR2581) and Landesgraduiertenförderung (to B. Berthet and A.M.).

AUTHOR CONTRIBUTIONS

H.T., M.A., and M.B. conceived the study. S.E., D.A., B.S., B. Bollhöner, H.H., and B. Berthet performed the experiments. A.M., M.B., S.E., B. Bollhöner, M.A., and H.T. supervised the experiments. S.E. and H.T. wrote the manuscript with help from all of the co-authors.

DECLARATION OF INTERESTS

The authors declare no competing interests.

Received: October 16, 2019
Revised: November 22, 2019
Accepted: November 26, 2019
Published: January 16, 2020

REFERENCES

1. Gokhale, R.H., and Shingleton, A.W. (2015). Size control: the developmental physiology of body and organ size regulation. Wiley Interdiscip. Rev. Dev. Biol. *4*, 335–356.
2. Harashima, H., and Schnittger, A. (2010). The integration of cell division, growth and differentiation. Curr. Opin. Plant Biol. *13*, 66–74.
3. Meyerowitz, E.M. (1997). Genetic control of cell division patterns in developing plants. Cell *88*, 299–308.
4. Mizukami, Y., and Fischer, R.L. (2000). Plant organ size control: AINTEGUMENTA regulates growth and cell numbers during organogenesis. Proc. Natl. Acad. Sci. USA *97*, 942–947.
5. Daneva, A., Gao, Z., Van Durme, M., and Nowack, M.K. (2016). Functions and regulation of programmed cell death in plant development. Annu. Rev. Cell Dev. Biol. *32*, 441–468.
6. Lockshin, R.A., and Williams, C.M. (1964). Programmed cell death—II. Endocrine potentiation of the breakdown of the intersegmental muscles of silkmoths. J. Insect Physiol. *10*, 643–649.
7. Olvera-Carrillo, Y., Van Bel, M., Van Hautegem, T., Fendrych, M., Huysmans, M., Simaskova, M., van Durme, M., Buscaill, P., Rivas, S., Coll, N.S., et al. (2015). A conserved core of programmed cell death indicator genes discriminates developmentally and environmentally induced programmed cell death in plants. Plant Physiol. *169*, 2684–2699.
8. Escamez, S., and Tuominen, H. (2014). Programmes of cell death and autolysis in tracheary elements: when a suicidal cell arranges its own corpse removal. J. Exp. Bot. *65*, 1313–1321.
9. Fendrych, M., Van Hautegem, T., Van Durme, M., Olvera-Carrillo, Y., Huysmans, M., Karimi, M., Lippens, S., Guérin, C.J., Krebs, M., Schumacher, K., and Nowack, M.K. (2014). Programmed cell death controlled by ANAC033/SOMBRERO determines root cap organ size in Arabidopsis. Curr. Biol. *24*, 931–940.
10. Escamez, S., and Tuominen, H. (2017). Contribution of cellular autolysis to tissular functions during plant development. Curr. Opin. Plant Biol. *35*, 124–130.
11. Fourquin, C., Beauzamy, L., Chamot, S., Creff, A., Goodrich, J., Boudaoud, A., and Ingram, G. (2016). Mechanical stress mediated by both endosperm softening and embryo growth underlies endosperm elimination in Arabidopsis seeds. Development *143*, 3300–3305.
12. Bell, J., and McCully, M.E. (1970). A histological study of lateral root initiation and development in Zea mays. Protoplasma *70*, 179–205.
13. Bonnett, H.T., Jr. (1969). Cortical cell death during lateral root formation. J. Cell Biol. *40*, 144–159.
14. Karas, I., and McCully, M.E. (1973). Further studies of the histology of lateral root development in Zea mays. Protoplasma *77*, 243–269.
15. Kosslak, R.M., Chamberlin, M.A., Palmer, R.G., and Bowen, B.A. (1997). Programmed cell death in the root cortex of soybean root necrosis mutants. Plant J. *11*, 729–745.
16. Malamy, J.E., and Benfey, P.N. (1997). Organization and cell differentiation in lateral roots of Arabidopsis thaliana. Development *124*, 33–44.
17. Stocking, C. (1956). Histology and development of the root. In Pflanze und Wasser/Water Relations of Plants, Handbuch der Pflanzenphysiologie/Encyclopedia of Plant Physiology, *Volume 3*, M.J. Adriani, et al., eds. (Springer), pp. 173–187.
18. Péret, B., Li, G., Zhao, J., Band, L.R., Voß, U., Postaire, O., Luu, D.-T., Da Ines, O., Casimiro, I., Lucas, M., et al. (2012). Auxin regulates aquaporin function to facilitate lateral root emergence. Nat. Cell Biol. *14*, 991–998.
19. Kumpf, R.P., Shi, C.-L., Larrieu, A., Stø, I.M., Butenko, M.A., Péret, B., Riiser, E.S., Bennett, M.J., and Aalen, R.B. (2013). Floral organ abscission peptide IDA and its HAE/HSL2 receptors control cell separation during lateral root emergence. Proc. Natl. Acad. Sci. USA *110*, 5235–5240.
20. Lucas, M., Kenobi, K., von Wangenheim, D., Voβ, U., Swarup, K., De Smet, I., Van Damme, D., Lawrence, T., Péret, B., Moscardi, E., et al. (2013). Lateral root morphogenesis is dependent on the mechanical properties of the overlaying tissues. Proc. Natl. Acad. Sci. USA *110*, 5229–5234.
21. Porco, S., Larrieu, A., Du, Y., Gaudinier, A., Goh, T., Swarup, K., Swarup, R., Kuempers, B., Bishopp, A., Lavenus, J., et al. (2016). Lateral root emergence in Arabidopsis is dependent on transcription factor LBD29 regulation of auxin influx carrier LAX3. Development *143*, 3340–3349.
22. Swarup, K., Benková, E., Swarup, R., Casimiro, I., Péret, B., Yang, Y., Parry, G., Nielsen, E., De Smet, I., Vanneste, S., et al. (2008). The auxin influx carrier LAX3 promotes lateral root emergence. Nat. Cell Biol. *10*, 946–954.
23. Vermeer, J.E., von Wangenheim, D., Barberon, M., Lee, Y., Stelzer, E.H., Maizel, A., and Geldner, N. (2014). A spatial accommodation by neighboring cells is required for organ initiation in Arabidopsis. Science *343*, 178–183.
24. Vissenberg, K., Martinez-Vilchez, I.M., Verbelen, J.-P., Miller, J.G., and Fry, S.C. (2000). In vivo colocalization of xyloglucan endotransglycosylase activity and its donor substrate in the elongation zone of Arabidopsis roots. Plant Cell *12*, 1229–1237.
25. Vermeer, J.E., and Geldner, N. (2015). Lateral root initiation in Arabidopsis thaliana: a force awakens. F1000Prime Rep. *7*, 32.
26. Vilches-Barro, A., and Maizel, A. (2015). Talking through walls: mechanisms of lateral root emergence in Arabidopsis thaliana. Curr. Opin. Plant Biol. *23*, 31–38.
27. Hierl, G., Vothknecht, U., and Gietl, C. (2012). Programmed cell death in Ricinus and Arabidopsis: the function of KDEL cysteine peptidases in development. Physiol. Plant. *145*, 103–113.
28. Balazadeh, S., Siddiqui, H., Allu, A.D., Matallana-Ramirez, L.P., Caldana, C., Mehrnia, M., Zanor, M.I., Köhler, B., and Mueller-Roeber, B. (2010). A gene regulatory network controlled by the NAC transcription factor ANAC092/AtNAC2/ORE1 during salt-promoted senescence. Plant J. *62*, 250–264.
29. Czabotar, P.E., Lessene, G., Strasser, A., and Adams, J.M. (2014). Control of apoptosis by the BCL-2 protein family: implications for physiology and therapy. Nat. Rev. Mol. Cell Biol. *15*, 49–63.
30. Dou, D., Kale, S.D., Wang, X., Chen, Y., Wang, Q., Wang, X., Jiang, R.H., Arredondo, F.D., Anderson, R.G., Thakur, P.B., et al. (2008). Conserved C-terminal motifs required for avirulence and suppression of cell death by Phytophthora sojae effector Avr1b. Plant Cell *20*, 1118–1133.
31. Evangelisti, E., Govetto, B., Minet-Kebdani, N., Kuhn, M.L., Attard, A., Ponchet, M., Panabières, F., and Gourgues, M. (2013). The Phytophthora parasitica RXLR effector penetration-specific effector 1 favours Arabidopsis thaliana infection by interfering with auxin physiology. New Phytol. *199*, 476–489.
32. Marhava, P., Hoermayer, L., Yoshida, S., Marhavý, P., Benková, E., and Friml, J. (2019). Re-activation of Stem Cell Pathways for Pattern Restoration in Plant Wound Healing. Cell *177*, 957–969.e13.
33. Marhavý, P., Montesinos, J.C., Abuzeineh, A., Van Damme, D., Vermeer, J.E., Duclercq, J., Rakusová, H., Nováková, P., Friml, J., Geldner, N., and Benková, E. (2016). Targeted cell elimination reveals an auxin-guided biphasic mode of lateral root initiation. Genes Dev. *30*, 471–483.
34. van den Berg, C., Willemsen, V., Hage, W., Weisbeek, P., and Scheres, B. (1995). Cell fate in the Arabidopsis root meristem determined by directional signalling. Nature *378*, 62–65.
35. van den Berg, C., Willemsen, V., Hendriks, G., Weisbeek, P., and Scheres, B. (1997). Short-range control of cell differentiation in the Arabidopsis root meristem. Nature *390*, 287–289.
36. Voß, U., Wilson, M.H., Kenobi, K., Gould, P.D., Robertson, F.C., Peer, W.A., Lucas, M., Swarup, K., Casimiro, I., Holman, T.J., et al. (2015). The circadian clock rephases during lateral root organ initiation in Arabidopsis thaliana. Nat. Commun. *6*, 7641.
37. Bollhöner, B., Zhang, B., Stael, S., Denancé, N., Overmyer, K., Goffner, D., Van Breusegem, F., and Tuominen, H. (2013). Post mortem function of AtMC9 in xylem vessel elements. New Phytol. *200*, 498–510.
38. Geldner, N., Dénervaud-Tendon, V., Hyman, D.L., Mayer, U., Stierhof, Y.D., and Chory, J. (2009). Rapid, combinatorial analysis of membrane

compartments in intact plants with a multicolor marker set. Plant J. *59*, 169–178.

39. Bozhkov, P., and Jansson, C. (2007). Autophagy and cell-death proteases in plants: two wheels of a funeral cart. Autophagy *3*, 136–138.
40. Escamez, S., Stael, S., Vainonen, J.P., Willems, P., Jin, H., Kimura, S., Van Breusegem, F., Gevaert, K., Wrzaczek, M., and Tuominen, H. (2019). Extracellular peptide Kratos restricts cell death during vascular development and stress in Arabidopsis. J. Exp. Bot. *70*, 2199–2210.
41. Kwon, S.I., Cho, H.J., Jung, J.H., Yoshimoto, K., Shirasu, K., and Park, O.K. (2010). The Rab GTPase RabG3b functions in autophagy and contributes to tracheary element differentiation in Arabidopsis. Plant J. *64*, 151–164.
42. Minina, E.A., Filonova, L.H., Fukada, K., Savenkov, E.I., Gogvadze, V., Clapham, D., Sanchez-Vera, V., Suarez, M.F., Zhivotovsky, B., Daniel, G., et al. (2013). Autophagy and metacaspase determine the mode of cell death in plants. J. Cell Biol. *203*, 917–927.
43. Furuta, K.M., Yadav, S.R., Lehesranta, S., Belevich, I., Miyashima, S., Heo, J.O., Vatén, A., Lindgren, O., De Rybel, B., Van Isterdael, G., et al. (2014). Plant development. Arabidopsis NAC45/86 direct sieve element morphogenesis culminating in enucleation. Science *345*, 933–937.
44. Escamez, S., André, D., Zhang, B., Bollhöner, B., Pesquet, E., and Tuominen, H. (2016). METACASPASE9 modulates autophagy to confine cell death to the target cells during Arabidopsis vascular xylem differentiation. Biol. Open *5*, 122–129.
45. Escamez, S., Bollhöner, B., and Tuominen, H. (2017). Quick histochemical staining methods to detect cell death in xylem elements of plant tissues. In Xylem: Methods and Protocols, M. de Lucas, and J.P. Etchells, eds. (Springer), pp. 27–36.
46. Van Durme, M., and Nowack, M.K. (2016). Mechanisms of developmentally controlled cell death in plants. Curr. Opin. Plant Biol. *29*, 29–37.
47. Gao, Z., Daneva, A., Salanenka, Y., Van Durme, M., Huysmans, M., Lin, Z., De Winter, F., Vanneste, S., Karimi, M., Van de Velde, J., et al. (2018). KIRA1 and ORESARA1 terminate flower receptivity by promoting cell death in the stigma of Arabidopsis. Nat. Plants *4*, 365–375.
48. Matallana-Ramirez, L.P., Rauf, M., Farage-Barhom, S., Dortay, H., Xue, G.-P., Dröge-Laser, W., Lers, A., Balazadeh, S., and Mueller-Roeber, B. (2013). NAC transcription factor ORE1 and senescence-induced BIFUNCTIONAL NUCLEASE1 (BFN1) constitute a regulatory cascade in Arabidopsis. Mol. Plant *6*, 1438–1452.
49. He, X.J., Mu, R.L., Cao, W.H., Zhang, Z.G., Zhang, J.S., and Chen, S.Y. (2005). AtNAC2, a transcription factor downstream of ethylene and auxin signaling pathways, is involved in salt stress response and lateral root development. Plant J. *44*, 903–916.
50. Turco, G.M., Rodriguez-Medina, J., Siebert, S., Han, D., Valderrama-Gómez, M.Á., Vahldick, H., Shulse, C.N., Cole, B.J., Juliano, C.E., Dickel, D.E., et al. (2019). Molecular Mechanisms Driving Switch Behavior in Xylem Cell Differentiation. Cell Rep. *28*, 342–351.e4.
51. Steffens, B., Kovalev, A., Gorb, S.N., and Sauter, M. (2012). Emerging roots alter epidermal cell fate through mechanical and reactive oxygen species signaling. Plant Cell *24*, 3296–3306.
52. Hong, J.H., Savina, M., Du, J., Devendran, A., Kannivadi Ramakanth, K., Tian, X., Sim, W.S., Mironova, V.V., and Xu, J. (2017). A Sacrifice-for-Survival Mechanism Protects Root Stem Cell Niche from Chilling Stress. Cell *170*, 102–113.e14.
53. Xuan, W., Band, L.R., Kumpf, R.P., Van Damme, D., Parizot, B., De Rop, G., Opdenacker, D., Möller, B.K., Skorzinski, N., Njo, M.F., et al. (2016). Cyclic programmed cell death stimulates hormone signaling and root development in Arabidopsis. Science *351*, 384–387.
54. Ameisen, J.C. (2002). On the origin, evolution, and nature of programmed cell death: a timeline of four billion years. Cell Death Differ. *9*, 367–393.
55. Kim, J.H., Woo, H.R., Kim, J., Lim, P.O., Lee, I.C., Choi, S.H., Hwang, D., and Nam, H.G. (2009). Trifurcate feed-forward regulation of age-dependent cell death involving miR164 in Arabidopsis. Science *323*, 1053–1057.
56. Feng, Z., Sun, X., Wang, G., Liu, H., and Zhu, J. (2012). LBD29 regulates the cell cycle progression in response to auxin during lateral root formation in Arabidopsis thaliana. Ann. Bot. *110*, 1–10.
57. Grebe, M., Xu, J., Möbius, W., Ueda, T., Nakano, A., Geuze, H.J., Rook, M.B., and Scheres, B. (2003). Arabidopsis sterol endocytosis involves actin-mediated trafficking via ARA6-positive early endosomes. Curr. Biol. *13*, 1378–1387.
58. Boisnard-Lorig, C., Colon-Carmona, A., Bauch, M., Hodge, S., Doerner, P., Bancharel, E., Dumas, C., Haseloff, J., and Berger, F. (2001). Dynamic analyses of the expression of the HISTONE:YFP fusion protein in arabidopsis show that syncytial endosperm is divided in mitotic domains. Plant Cell *13*, 495–509.
59. Kubo, M., Udagawa, M., Nishikubo, N., Horiguchi, G., Yamaguchi, M., Ito, J., Mimura, T., Fukuda, H., and Demura, T. (2005). Transcription switches for protoxylem and metaxylem vessel formation. Genes Dev. *19*, 1855–1860.
60. Karimi, M., Inzé, D., and Depicker, A. (2002). GATEWAY vectors for Agrobacterium-mediated plant transformation. Trends Plant Sci. *7*, 193–195.
61. Clough, S.J., and Bent, A.F. (1998). Floral dip: a simplified method for Agrobacterium-mediated transformation of *Arabidopsis thaliana*. Plant J. *16*, 735–743.
62. Marhavý, P., and Benková, E. (2015). Real-time analysis of lateral root organogenesis in Arabidopsis. Bio Protoc. *5*, e1446.
63. Ötvös, K., Miskolczi, P., Marhavý, P., Cruz-Ramírez, A., Benková, E., Robert, S., and Bakó, L. (2019). PICKLE recruits RETINOBLASTOMA RELATED 1 to Control Lateral Root Formation in Arabidopsis. bioRxiv. https://doi.org/10.1101/643122.
64. Stangner, T., Dahlberg, T., Svenmarker, P., Zakrisson, J., Wiklund, K., Oddershede, L.B., and Andersson, M. (2018). Cooke-Triplet tweezers: more compact, robust, and efficient optical tweezers. Opt. Lett. *43*, 1990–1993.
65. Zakrisson, J., Singh, B., Svenmarker, P., Wiklund, K., Zhang, H., Hakobyan, S., Ramstedt, M., and Andersson, M. (2016). Detecting bacterial surface organelles on single cells using optical tweezers. Langmuir *32*, 4521–4529.
66. Henriksen, G.H., and Assmann, S.M. (1997). Laser-assisted patch clamping: a methodology. Pflugers Arch. *433*, 832–841.
67. Carmer, S.G., and Swanson, M.R. (1973). An evaluation of ten pairwise multiple comparison procedures by Monte Carlo methods. J. Am. Stat. Assoc. *68*, 66–74.

STAR★METHODS

KEY RESOURCES TABLE

REAGENT or RESOURCE	SOURCE	IDENTIFIER
Bacterial and Virus Strains		
Escherichia coli strain DH5α	Widely distributed	N/A
Escherichia coli strain DB3.1	Widely distributed	N/A
Agrobacterium tumefaciens strain GV3101 pMP90	Widely distributed	N/A
Chemicals, Peptides, and Recombinant Proteins		
Murashige and Skoog (MS) medium (including vitamins)	Duchefa Biochemie	M0222
Fluorescein diacetate	Merck	F7378
Propidium iodide	Merck	P4864-10ML
Triton X-100	Merck	11332481001
X-Gluc	Thermo Fisher	R0851
Potassium hexacyanoferrate(III) ($K_3Fe(CN)_6$)	Merck	244023
Potassium hexacyanoferrate(II) ($K_4Fe(CN)_{6)}$	Merck	455989
Chloral hydrate	Merck	15307
PhytagelTM	Merck	P8169-250G
MES	Merck	M1317
Glutaraldehyde	Merck	G5882
Osmium tetroxide	Merck	75632
Propylene oxide	Merck	82320
Spurr's resin	Polysciences	01916-1
Uranyl acetate	Agar scientific	AGR1260A
Lead Acetate	Agar scientific	AGR1209
Chloramphenicol	Merck	C0378-25G
Spectinomycin	Merck	S4014-5G
Critical Commercial Assays		
Gateway BP Clonase II Enzyme mix	Thermo Fisher	11789100
Gateway LR Clonase II Enzyme mix	Thermo Fisher	11791100
RNeasy Plant Kit	QIAGEN	74904
RNase-Free DNase Set	QIAGEN	79254
QuantiTect Reverse Transcription Kit	QIAGEN	205311
LightCycler® 480 SYBR Green I Master Mix	Roche	04707516001
Deposited Data		
LRP growth transcriptomics data from Voß et al. (2015)	ArrayExpress	E-MTAB-2565
Experimental Models: Organisms/Strains		
Arabidopsis thaliana (*Arabidopsis*) Columbia-0 (col-0) ecotype, wild-type	NASC	N1092
Arabidopsis Wassilewskija (Ws) ecotype, wild-type	NASC	N5390
Arabidopsis anac092-1 mutant	NASC & [28]	SALK_090154
Arabidopsis ore1-2 mutant	NASC & [55]	N/A
Arabidopsis bfn1-1 mutant	NASC & [9]	GK-197G12
Arabidopsis bfn1-2 mutant	NASC	SALK_017287
Arabidopsis mc9-1 mutant	NASC & [37]	GABI_540_H06
Arabidopsis mc9-2 mutant	NASC & [37]	SALK_075814
Arabidopsis mutant for *DMP4*	NASC	SALK_063946
Arabidopsis mutant for *EXI1*	NASC	SALK_137383
Arabidopsis mutant for *EXI1*	NASC	SAIL_760_G07

(*Continued on next page*)

Continued

REAGENT or RESOURCE	SOURCE	IDENTIFIER
Arabidopsis lbd29 mutant	NASC & [56]	SALK_071133C
Arabidopsis 35S::SRDX:LBD29 dominant suppressor line	NASC & [21]	N/A
Arabidopsis mutant for *RNS3*	NASC	FLAG_164_A04
Arabidopsis pro*DMP4::GUS*	This study	N/A
Arabidopsis pro*RNS3::GUS*	This study	N/A
Arabidopsis pro*BFN1::GUS*	This study	N/A
Arabidopsis pro*MC9::MC9:GUS*	[37]	N/A
Arabidopsis pro*ORE1::GUS*	[28]	N/A
Arabidopsis pro*BFN1::ToIM*	This study	N/A
Arabidopsis pro*UBQ10::WAVE131:YFP*	[38]	N/A
Arabidopsis pro*CASP1::CIT:SYP122*	[23]	N/A
Arabidopsis pro*BFN1::nucGFP*	[37]	N/A
Arabidopsis pro*UBQ10::WAVE131:YFP* pro*BFN1::nucGFP*	This study	N/A
Arabidopsis pro*CASP1::CIT:SYP122* pro*BFN1::nucGFP*	This study	N/A
Arabidopsis 35S::GFP:LTi6a	[57]	N/A
Arabidopsis 35S::H2B:YFP	[58]	N/A
Arabidopsis 35S::GFP:LTi6a 35S::H2B:YFP	This study	N/A
Arabidopsis pro*ATG8a::GFP:ATG8a*	[43]	N/A
Arabidopsis pro*BFN1::mBAX* (Col-0 background)	This study	N/A
Arabidopsis ore1-2 pro*BFN1::mBAX* lines 1-6	This study	N/A
Oligonucleotides		
For Gateway cloning of *DMP4* promoter: proAT4G18425-attB1 (Forward), GGGGACAAGTTTGTACAAAAAAGCAGGCTTACCG AACTGATCAAACATATATGATC; attB2-proAT4G18425 (Reverse), GGGGACCACTTTGTACAAGAAAGCTGGGTAATCTTTGAAGTT GTTTCCTTTGTC	This study (synthesis ordered from Thermo Fisher)	N/A
For Gateway cloning of *RNS3* promoter: proAT1G26820-attB1 (Forward), GGGGACAAGTTTGTACAAAAAAGCAGGCTTAGG AGAAGAAGAAGAGGACAGACC; attB2-proAT1G26820 (Reverse), GGGGACCACTTTGTACAAGAAAGCTGGGTATTCCTCAAGAT ATCAAATAATTTG	This study (synthesis ordered from Thermo Fisher)	N/A
For Gateway cloning of *BFN1* promoter: proAT1G11190-attB1 (Forward)GGGGACAAGTTTGTACAAAAAAGCAGGCTTAATCAA TGGTATAGATTTG attB2-proAT1G11190 (Reverse)GGGGACC ACTTTGTACAAGAAAGCTGGGTAATCTTCAAAGTTTGAAACTTA	This study (synthesis ordered from Thermo Fisher)	N/A
For checking expression of *EXI1* Forward: ATGATGTATCTAAGTCGGAGA Reverse: TTAGTGGCGTGAAGGC	This study (synthesis ordered from Thermo Fisher)	N/A
For checking expression of *RNS3* Forward: AATTCTTCATTTTTATTCTAGCGT Reverse: TTAGAACTTGGGAAATTGAACT	This study (synthesis ordered from Thermo Fisher)	N/A
For checking expression of *DMP4* (5' end of transcript)Forward: TGACGAAGGTCATCAAAAAGG Reverse: TAGAAGCTGAAACGCGAGAA	This study (synthesis ordered from Thermo Fisher)	N/A
For checking expression of *DMP4* (3' end of transcript) Forward: TTGGTGCGGTGGTTTTATTC Reverse: CAATCCCATTGCGTGTTGT	This study (synthesis ordered from Thermo Fisher)	N/A

(*Continued on next page*)

Continued

REAGENT or RESOURCE	SOURCE	IDENTIFIER
For checking expression of *BFN1* Forward: CCCTTTTGTTCTTGTCTCATTTC Reverse: ACGCCTTTGTATCCCCATTT	This study (synthesis ordered from Thermo Fisher)	N/A
For checking expression of *ORE1* (full length) Forward: ATGGATTACGAGGCATCAAG Reverse: ATGGATTACGAGGCATCAAG	This study (synthesis ordered from Thermo Fisher)	N/A
For checking expression of *ORE1* (3' end of transcript) Forward: CAGAAGCCGGTTATTGGAAA Reverse: CGTTTTTGGAAAACACGACA	This study (synthesis ordered from Thermo Fisher)	N/A
For checking expression of *mBAX* (full length) Forward: ATGGACGGGTCCGGGGAGCAG Reverse: TCAGCCCATCTTCTTCCAGAT	This study (synthesis ordered from Thermo Fisher)	N/A
For checking expression of *mBAX* (3' end of transcript, for qPCR) Forward: TGCAGAGGATGATTGCTGAC Reverse: GATCAGCTCGGGCACTTTAG	This study (synthesis ordered from Thermo Fisher)	N/A
For checking expression of *UBQ10* (3' end of transcript, reference gene for qPCR) Forward: GGCCTTGTATAATCCCTGATGAATAAG Reverse: AAAGAGATAACAGGAACGGAAACATAGT	This study (synthesis ordered from Thermo Fisher)	N/A
For checking expression of *CESA8/IRX1* (3' end of transcript, for qPCR) Forward: GGTTCTACGTTGGGCTCTTG Reverse: ATACTGACTCCGCTCCATCG	This study (synthesis ordered from Thermo Fisher)	N/A
For genotyping of SALK_063946 (for *DMP4*) Forward: GAACTTCCAATGCTTCTGCTGReverse: TGTCATTGACAAATGACACGG	This study (synthesis ordered from Thermo Fisher)	N/A
For genotyping of SALK_017287 (*bfn1-2*) Forward: TAAACAAAGCAGTCCACAGGCReverse: TGGTTTAAGATTGGCTTGACG	This study (synthesis ordered from Thermo Fisher)	N/A
For genotyping of SALK_137383 (for *EXI1*) Forward: ACTTTTTCCACCTGCAATTTGReverse: CATCTATGAATCCATGTCCGG	This study (synthesis ordered from Thermo Fisher)	N/A
For genotyping of SAIL_760_G07 (for *EXI1*) Forward: ACATCTTTCATTTGCATTGGCReverse: AAGGTTAGATTGCGTATTATTTTGG	This study (synthesis ordered from Thermo Fisher)	N/A
For genotyping of FLAG_164_A04 (for *RNS3*) Forward ("Left primer" regarding the orientation of the T-DNA): CATGCCTTGAATTTCAGCAAGReverse ("Right primer" regarding the orientation of the T-DNA): GCCCAAGATTTCGATTTCTTC	This study (synthesis ordered from Thermo Fisher)	N/A

(*Continued on next page*)

Continued

REAGENT or RESOURCE	SOURCE	IDENTIFIER
Recombinant DNA		
pENTR207	Thermo Fisher (formerly invitorgen)	N/A (no longer sold by this manufacturer)
pBGGUS	[59]	N/A
pro*DMP4::GUS*	This study	N/A
pro*RNS3::GUS*	This study	N/A
pro*BFN1::GUS*	This study	N/A
pro*MC9::MC9:GUS*	[37]	N/A
pro*ORE1::GUS*	[28]	N/A
pDONR P4P1r	Thermo Fisher (formerly invitrogen)	N/A (no longer sold by this manufacturer)
pK7m34GW-*pPASPA3-eGFP-2A-sp-mRFP*	[9]	N/A
pK7m34GW-pBFN1-eGFP-2A-sp-mRFP	This study	N/A
pro*BFN1::ToIM*	This study	N/A
pENTRL4R1 containing the *proBFN1* fragment (pENTRL4R1-pBFN1)	This study	N/A
pENTR221 containing the *mBAX* gene	Dr. Moritz Nowack (VIB Gent; unpublished)	N/A
pK7m24GW	[60]	N/A
pro*BFN1::mBAX*	This study	N/A
Software and Algorithms		
ImageJ/Fiji	N/A	https://imagej.net/Fiji
Minitab 17	Minitab LLC	https://www.minitab.com/en-us/products/minitab/
Other		
Glass capillaries, 1.8 mm of diameter, 100µl	Blaubrand intraMark	7087 44
Nunc™ Lab-Tek™ 1-well microscopy Chamber	Thermo Fisher	155361

LEAD CONTACT AND MATERIALS AVAILABILITY

This study did not generate new unique reagents or resources, but new materials such as *Arabidopsis* transgenic lines were generated in this study. These materials will be made available upon request addressed to the Lead Contact, Dr. Hannele Tuominen (hannele.tuominen@umu.se).

EXPERIMENTAL MODEL AND SUBJECT DETAILS

Plant Material

The model plant species *Arabidopsis thaliana* (*Arabidopsis*) has been used throughout this study. Most of the *Arabidopsis* knock-out mutant plants used in this study are in the Columbia-0 (Col-0) genetic background, and were therefore compared with a Col-0 wild-type: *anac092-1* (*ore1* allele SALK_090154 [28];), *ore1-2* (5bp deletion [55];), *bfn1-1* (GK-197G12 [9];), *bfn1-2* (SALK_017287), *mc9-1* (GABI_540_H06 [37];), *mc9-2* (SALK_075814 [37];), SALK_063946 (for *DMP4*), SALK_137383 and SAIL_760_G07 (for *EXI1*). The knock-out mutant *lbd29* (SALK_071133C) and the dominant suppressor *35S::SRDX:LBD29* were also in the Col-0 background, generated in previous studies [56]. The FLAG_164_A04 knock-out mutant (for *RNS3*) in the Wassilewskija (Ws) genetic background was compared to Ws wild-type.

The transcriptional reporter lines for histological detection of promoter activity were either generated in this study (pro*DMP4::GUS*, pro*RNS3::GUS* and pro*BFN1::GUS*, as described in the "Method Details" below), or obtained from previous studies (pro*MC9::MC9:GUS* from [37] and pro*ORE1::GUS* from [28]).

The *BFN1* promoter-driven fluorescent tonoplast integrity marker (pro*BFN1::ToIM*) to monitor cell death was created in this study (as described in "Method Details" below) based on a previously published construct [9]. The double markers for fluorescently labeled plasma membranes (ubiquitous: pro*UBQ10::WAVE131:YFP*; or endodermis-specific: pro*CASP1::CIT:SYP122*) and *BFN1* promoter-driven nuclear GFP (pro*BFN1::nucGFP*) were generated in this study by crossing previously generated individual markers [23, 37, 38]. The double marker for ubiquitous fluorescent labeling of both plasma membranes (*35S::GFP:LTi6a*) and nuclei (*35S::H2B:YFP*) were also generated in this study by crossing previously generated individual markers [57, 58]. The autophagy reporter pro*ATG8a::GFP:ATG8a* had been generated previously [43].

Growth conditions

To compare the speed of LRE between genotypes, seedlings were grown on ½ MS medium for three days in constant light (150 $\mu E \cdot m^{-2} \cdot s^{-1}$) on vertical plates, which were then rotated 90° to induce LRP initiation [18]. For laser ablation, seedlings were transferred to sterile microscopy chambers and covered with a slab of the medium they had been growing on, to allow them to continue growing within the chamber over the course of LRP growth.

Seedlings for observations of naturally initiated LRPs (no gravitational induction) were grown on ½ MS medium for 3.5 - 7 days after germination in 16 h day (150 $\mu E \cdot m^{-2} \cdot s^{-1}$) / 8 h night cycles.

Genotypes meant to be compared always consisted of seeds that had been harvested at the same time, from plants grown in the same location and conditions.

METHOD DETAILS

BFN1 co-expression analysis

To identify genes correlating in expression with *BFN1* during LR development, smooth splines were fitted through the transcriptomic profiles for all genes, to smooth out the noise. The Pearson correlation between each gene's profile and that of the target gene *BFN1* was calculated, including all data points, i.e., not just mean values for each time point. Genes were ranked in decreasing order of the Pearson correlation with *BFN1* (Table S1).

Cloning and plant transformation

For promoter-reporter constructs, 1654 bp (AT4G18425; *DMP4*) or 2000 bp (AT1G26820; *RNS3*) upstream of the translational start codon were amplified and recombined by Gateway-mediated cloning via pENTR207 (Invitrogen) into the destination vector pBGGUS [59]. pro*BFN1::GUS* was obtained by recombining a 670 bp promoter region of *BFN1* (AT1G11190) into pMDC163. Col-0 plants were transformed with *Agrobacterium tumefaciens* using the floral dip method [61]. At least five independent lines were analyzed for each construct to select representative lines. pro*BFN1::*nuc*GFP* and pro*MC9::MC9:GUS* have been described previously [37].

To place the tonoplast integrity marker (ToIM [9];) downstream of the *BFN1* promoter, the promoter of the putative protease *PASPA3* previously cloned upstream of the tonoplast integrity marker [9] was replaced by the *BFN1* promoter. To do so, the *BFN1* promoter was amplified from a plasmid using primers comprising the attB4 and attB1r sequences, and recombined into pDONR P4P1r. The *PASPA3* promoter from pK7m34GW-*pPASPA3-eGFP-2A-sp-mRFP* [9] was removed by a standard BP recombination with pDONRP4P1r, the destination vector was recovered by selecting on Chloramphenicol and Spectinomycin in DB3.1 cells and subsequently recombined during an LR reaction with pENTRL4R1-pBFN1. The resulting expression vector pK7m34GW-pBFN1-eGFP-2A-sp-mRFP was used to electroporate *Agrobacterium tumefaciens*. Agrobacterium-mediated floral dip transformation of wild-type (Col-0) plants was performed and several apparent transformants were screened for visible ToIM signal, leading to the selection of a representative pro*BFN1::ToIM* marker line.

To express the cell death agonist mammalian protein mBAX under the transcriptional control of the *BFN1* promoter, the vectors pENTRL4R1 containing the *proBFN1* fragment and pENTR221 containing the *mBAX* gene (a kind gift from Moritz Nowack) were together recombined into pK7m24GW [60] using standard protocols for LR recombination. This vector was transferred into *Agrobacterium tumefaciens* to transform Col-0 and *ore1-2* plants by floral dip. Transformants were then screened to identify homozygous lines in each genotype displaying *mBAX* expression.

Gravitational induction of LRP initiation

Determination of LRP stage was performed 18h and 42h after synchronized LR induction by gravitational stimulus, as described previously [16, 18]. Briefly, the seedlings were fixed and cleared by a 15 min incubation in acidified methanol (20% v/v methanol with 4% v/v HCl), followed by 15 min in 60% v/v ethanol mixed with 7% v/v NaOH, and 5 min steps in an ethanol gradient (40%, 20% and 10% v/v ethanol). The fixed and cleared seedlings were then mounted in 50% glycerol and observed as described in ''light microscopy'' below.

In the specific case of laser-assisted cell elimination experiments, the seedlings were not fixed or cleared but directly observed inside of the microscopy chambers where they were growing, similar to a previously published method real time analysis of lateral root organs [62].

Confocal Laser Scanning Microscope analyses

All time-lapses with cLSM were acquired using a Zeiss LSM780 inverted microscope, by placing the seedlings in microscope chambers as previously described [62]. GFP and CITRINE signals (Figures 2 and S1D–S1H) were simultaneously recorded with a spectral detector after excitation with a 488 nm laser line, and separated by online fingerprinting (i.e., unmixing which occurs during, rather than after, acquisition). eGFP and mRFP signals (Video S4) from the ToIM marker [9] were detected simultaneously upon excitation with 488 nm (for eGFP) and 561 nm (for mRFP) laser lines.

cLSM micrographs that are not part of any time-lapse were acquired either with a Zeiss LSM780, an upright Zeiss LSM800 or an inverted Zeiss LSM880 microscope. For FDA and PI staining, 3.5-4 days old *Arabidopsis* seedlings were incubated for 1h in liquid ½ MS medium containing 10 μg/mL PI and 12 nM FDA, and imaged as similarly to the ToIM maker (described above), as previously described [44].

Transmission electron microscopy

An early-stage LRP marker pro*LBD16*::*GFP* line [63] was used to identify regions of the root containing primordia. Tissues were fixed under vacuum in 2.5% w/v glutaraldehyde in 0.1 M Na cacodylate buffer, pH7.3 for 30 min, and then without vacuum overnight at 4°C. Tissues were then stained with 1% w/v osmium tetroxide for 2 h at room temperature in the dark, washed twice in water, and then dehydrated in 15-minute steps through an ethanol series (50, 70, 90, and 100%). Root portions were then rinsed in propylene oxide and exchanged with Spurr's resin (Polysciences) and then baked at 65°C for 2 days. Sections were mounted on formvar-coated copper grids. Contrasting was done for 45 min in 5% uranyl acetate followed by 5 min in Sato's lead acetate staining.

Light microscopy

All observations were performed with an upright Zeiss Axioplan II microscope or with an inverted Leica DMi8, both equipped for epifluorescence microscopy.

Histochemical GUS assays were performed as described previously [37]. Briefly, 3.5-5 days old transgenic seedlings were incubated for 1h-18h at 37°C in a solution consisting of 1 mM X-Gluc, 1 mM $K_3Fe(CN)_6$, 1 mM $K_4Fe(CN)_6$ and 0.1% Triton x-100 in 50 mM sodium phosphate buffer (pH7). After this, the samples were cleared in 70% ethanol and rehydrated in an ethanol gradient in 5 min steps (50%, 40%, 20% and 10% v/v ethanol), followed by additional clearing in a chloral hydrate solution (chloral hydrate/glycerol/H2O 8:2:3 v/v) for at least 1 h. The samples were mounted in 50% glycerol and observed using differential interference contrast [16].

LRP of seedlings harboring the pro*BFN1::*nuc*GFP* constructs were observed while alive following mounting in liquid ½ MS medium. Both differential interference contrast and fluorescence micrographs were acquired to relate the possible presence of nucGFP signal to the LRP stage.

Lightsheet fluorescence microscopy

Seeds were sterilized for 10min with 70% ethanol supplemented with 0.05% Triton X-100, washed 3 times with 70% ethanol, and incubated for 10 min with 100% ethanol before being dried out under the sterile bench. Glass capillaries (1.8 mm of diameter, Blaubrand intraMark, glass micropipettes 100 μL Ref. 7087 44) were sterilized with 70% ethanol for 20 min, then 100% ethanol for 20 min and left to dry. The capillaries were filled with ½ MS medium buffered with 0.5 g/L MES (adjusted to pH 5,8 with KOH), containing 1% (m/V) of Phytagel (Sigma Phytagel™ P8169-250G) and placed in a small round plate filled with the same medium. One seed was placed on top of each capillary and stratified for 48h before transfer to long day conditions for 4 to 5 days at 22°C.

Imaging was performed on a Luxendo MuViSPIM, equipped with two-sided illumination and two cameras for detection. In the microscope, the plant was continuously illuminated (red and blue LEDs, turned off during stack acquisition) and the temperature was maintained at 24°C. About 5 mm of the root surrounded by a cylinder of Phytagel medium was extruded out of the glass capillary which itself was positioned vertically in the microscope's chamber containing liquid, sterile ½ MS medium. The shoots of the seedling were left out of the liquid medium.

Samples were excited by a 488 nm laser light sheet (2.5 μm thickness at the waist) generated with Nikon Plan Fluor 10X/0.30W objectives. Laser power was kept < 6 mW. The emitted fluorescence was detected by Nikon Apo 40X/0.80W DIC N2 objectives associated with a 497-553 nm band pass filter and captured using 2 Hamamatsu Orca-flash 4.0 cameras with an exposure time < 100 ms. Under these conditions, both reporters (cell death marker pro*BFN1::*nuc*GFP* and plasma membrane marker pro*CASP1::CITRINE:SYP122*) were collected in the same channel. Stacks were acquired every 10 min for 24 h with a z-step of 0.250 μm spanning a total volume of 200 μm containing the growing LRP and the primary root overlying tissues. Due to drifting of the samples in the liquid medium, a total of only two successful observations could be performed (two LRP, each from a different seedling).

After fusion of the two opposite views with the proprietary script of Luxendo, sample drift was corrected using the BigDataTracker plugin in ImageJ (Fiji).

Laser-assisted targeted cell elimination

Laser ablation was conducted with the same aim as previous studies which successfully caused the death of single cells in *Arabidopsis* roots [32–35], but with an experimental setup relying on the so called optical tweezers technique. To cause deadly wounds specifically to LRP-overlying endodermal cells, we used a modified inverted microscope (IX71, Olympus) normally utilized in optical tweezers applications [64]. A Gaussian laser beam (TEM00, M2 < 1.1) from a continuous wavelength laser (Rumba, 05-01 Series, Cobolt AB) operating at 1064 nm was introduced into the microscope. We used a 60x water immersion objective (UPlanSApo, Olympus), with a numerical aperture of 1.2 and a working distance of 0.28 mm to focus the beam and create a high-intensity spot. To perform accurate positioning of the laser focal spot we aligned the beam so the focal spot coincides with the focal plane of the microscope objective. A diffraction-limited spot of ~560 nm and a depth of field of ~300 nm was created that we could position with nm-resolution in the lateral and axial plane using a combination of micro-attenuators and a piezo stage (PI-P5613CD, Physik Instruments) [65]. Since the objective strongly focused the laser beam ~65°, the intensity dropped fast from the focal spot, both in the lateral and axial directions, making ablation limited to only one specific cell [66]. We estimated the intensity in the focal spot to 2.48 MW/mm^2 by measuring the effective power (1490 mW) before the objective and by taking into account the parameter values (transmission, focal length, etc.) of the objective specified by the manufacturer. Finally, we visualized and imaged plants mounted in microscopy chamber (1-well Lab-Tek chamber, Nunc) as previously described [62] using a CCD camera (C11440-10C, HAMAMATSU, 8 bit).

RNA isolation and qPCR

For quantitative real-time PCR analyses, *Arabidopsis* seedlings of the indicated genotypes were grown for 5 days as indicated above for naturally initiated LRP. For each genotype, 10 seedlings were pooled together and ground in liquid nitrogen. RNA extraction on these ground samples was performed using RNeasy Plant Kit (QIAGEN), including "on column DNase treatment," following manufacturer's instruction. RNA concentration was measured with Nanodrop and all samples were diluted to 100 ng/μL. 500 ng of total RNA were used for cDNA synthesis using QuantiTect Reverse Transcription Kit (QIAGEN), including gDNase treatment (for the second time) prior to cDNA synthesis. cDNA samples were diluted 25 times and 5 μL were used as template in a 20 μL total reaction volume, using LightCycler 480 SYBR Green 1 Master (Roche Life Science) according to the manufacturer's instructions. Each sample was loaded in duplicate into a 96-well qPCR plate (Roche Life Science) and qPCR was run in a LightCycler 480 thermal cycler (Roche Life Science) for 45 cycles (initial denaturation at 98°C for 3 min, cycling: denaturation at 95°C for 5 s, annealing at 55°C for 10 s, elongation at 72°C for 30 s; melting curve from 45°C to 95°C with acquisitions every 1°C).

QUANTIFICATION AND STATISTICAL ANALYSIS

Statistical analyses

For multiple comparison of continuous variables (e.g., root length, lateral root density, frequency of cell death…) between genotypes, post-ANOVA Fisher LSD tests were performed using Minitab 17, provided that the ANOVA indicated significant overall differences ($p < 0.05$). The choice of this test is justified because statistical studies have shown that under the condition of an ANOVA returning $p < 0.05$, the post-ANOVA Fisher LSD test provides the best detection of true pairwise differences, while performing as well or better than other tests (e.g., Tukey's test) against type I error [67].

For comparisons of stages of LRP growth, which is a categorical variable (each stage is a category, and the variable is not continuous but discrete) we opted for the Chi-square test because it allows to test whether two categorical variables are independent from one another. For instance, we tested whether the categorical variable "LRP stage" and the categorical variable "genotype" were independent (H_0) or not (H_1). If the distribution LRP stage is not independent from genotype (i.e., if $p < 0.05$), then the conclusion is that the compared genotypes have significantly different LRP growth speed.

All charts displaying values as bars show averages of several replicate experiments (number of combined replicate experiments and of biological replicates are indicated in the figure legends), and error bars always represent standard error of the mean (SEM).

DATA AND CODE AVAILABILITY

Neither custom code nor datasets were generated in this study. Transcriptomics results presented in this study rely on a previously published dataset [36].